Stress-activated constraints in dense suspension rheology

Abhinendra Singh, Grayson L. Jackson, Michael van der Naald, Juan J. de Pablo, and Heinrich M. Jaeger

Phys. Rev. Fluids **7**, 054302 — Published 27 May 2022

DOI: 10.1103/PhysRevFluids.7.054302

Stress-activated Constraints in Dense Suspension Rheology

Abhinendra Singh,[1,2,*] Grayson L. Jackson,[1] Michael van der Naald,[1,3] Juan J de Pablo,[2,4] and Heinrich M Jaeger[1,3]

[1] *James Franck Institute, University of Chicago, Chicago, Illinois 60637, USA*
[2] *Pritzker School of Molecular Engineering, University of Chicago, Chicago, Illinois 60637, USA*
[3] *Department of Physics, The University of Chicago, Chicago, Illinois 60637, USA*
[4] *Materials Science Division, Argonne National Laboratory, Lemont, Illinois 60439, USA*

(Dated: May 13, 2022)

Dispersing small particles in a liquid can produce surprising behaviors when the solids fraction becomes large: rapid shearing drives these systems out of equilibrium and can lead to dramatic increases in viscosity (shear thickening) or even solidification (shear jamming). These phenomena occur above a characteristic onset stress when particles are forced into frictional contact. Here we show via simulations how this can be understood within a framework that abstracts details of the forces acting at particle-particle contacts into general stress-activated constraints on relative particle movement. We find that focusing on just two constraints, affecting sliding and rolling at contact, can reproduce the experimentally observed shear thickening behavior quantitatively, despite widely different particle properties, surface chemistries, and suspending fluids. Within this framework parameters such as coefficients of sliding and rolling friction can each be viewed as proxy for one or more forces of different physical or chemical origin, while the parameter magnitudes indicate the relative importance of the associated constraint. In this way, a new link is established that connects features observable in macroscale rheological measurements to classes of constraints arising from micro- or nano-scale properties.

I. INTRODUCTION

Concentrated or "dense" suspensions comprising small particles in a suspending liquid are ubiquitous in nature as well as industrial settings [1–5]. Even for simple liquids with completely Newtonian characteristics, i.e. constant viscosity, such suspensions can exhibit strikingly non-Newtonian behaviors under applied shear, such as yielding, shear thinning, shear thickening, and shear-jamming [4–9]. All of these behaviors originate from short-ranged forces between particles that either are mediated by the hydrodynamics of thin liquid layers or involve direct, frictional and possibly also cohesive contact [10–12]. The strength of these forces depends not only on the particles' physical properties such as shape, stiffness and surface roughness, but also on their surface chemistry and its role during particle-particle contact or through interaction with the surrounding liquid [13–17]. Given this large set of potentially contributing factors, establishing a predictive link between microscale properties and macroscale observable flow behaviors has been a longstanding problem.

One recent approach, by Guy *et al.*, to address this issue has been to classify the macroscale rheology not by focusing on the details of specific forces, but rather on the general types of constraints that affect relative particle movement [18]. The promise of this approach lies in that the physical or chemical origin of any particular particle-particle interaction may matter far less than its net effect on the ability of neighboring particles to move with respect to one another. What remained to be shown, however, is which specific types of constraints are necessary for quantitative modeling of dense suspension rheology.

Here we demonstrate that quantitative modeling and prediction is indeed possible. We focus on shear thickening, perhaps the most remarkable non-Newtonian behavior of dense suspensions, and introduce a new diagnostic framework to classify rheological flow curves in terms of whether sliding and rolling constraints on particle motion are present. This approach provides insight into why particular particle-scale properties introduce additional constraints while others do not and unlocks a new connection between bulk rheology and nanoscale particle surface properties (Fig. 1A).

During shear thickening the shear stress σ increases faster than the shear rate $\dot{\gamma}$, leading to a net increase in viscosity $\eta = \sigma/\dot{\gamma}$. For low solids volume fractions ϕ this increase is mild and occurs continuously as a function of applied shear, but for larger ϕ the viscosity can increase abruptly and dramatically when a critical rate $\dot{\gamma}_c$ is reached, behavior termed discontinuous shear thickening (DST). For sufficiently large ϕ and shear stress σ, these suspensions can furthermore transform into a shear-jammed (SJ), solid-like state, which "melts" back into a fluid once stress is released [19, 20]. Past work has established a strong foundation to understand the evolution of shear thickening toward DST and SJ, yet focused almost exclusively on stress-activated sliding friction, represented by a single coefficient for sliding friction μ_s.

In this picture, once the applied shear stress overwhelms the repulsive interparticle potential, unconstrained, hydrodynamically "lubricated" contacts transition to "frictional" contacts that prevent sliding [11–13, 21–26]. When viscosity η is plotted as a function

* abhinendra@uchicago.edu

of applied shear stress σ (Fig. 1B), this increase in the number of frictionally constrained particle-particle contacts manifests as shear thickening that starts at an onset stress $\sigma_{\rm on}$ and persists up to an upper limit $\sigma_{\rm max}$, where the system has reached a state with all contacts frictional. As the solids fraction ϕ gets closer to the onset packing fraction for jamming ϕ_J^μ, the dependence of η on stress becomes steeper within the shear thickening regime, until DST is reached. In plots like Fig. 1B, DST is identified by a slope $d(\log\eta)/d(\log\sigma) = 1$, i.e., the viscosity $\eta = \sigma/\dot{\gamma}_c$ is directly proportional to the stress. Increasing the sliding friction coefficient μ_s reduces ϕ_J^μ and thus, for given ϕ, brings the system closer to jamming. This in turn steepens the rise in viscosity with stress while at the same time increasing the final viscosity level that is reached in the large stress limit.

However, if only sliding constraints are considered, the effect of μ_s on ϕ_J^μ is modest: it reduces the onset of jamming from ϕ_J^0 for frictionless ($\mu_s = 0$) particles, which for monodisperse rigid spheres is equal to the random close-packing value $\phi_{\rm RCP} \approx 0.64$ [18, 22, 25, 27], to no lower than $\phi_J^\mu \approx 0.56$ even for $\mu_s = \infty$ [22, 25]. This poses a serious problem for quantitative prediction, since experiments with rough spherical particles and also with specific chemical surface groups have demonstrated DST for packing fractions so low that the associated ϕ_J^μ lies well below 0.56 and thus outside the range of current models based on just μ_s [12–14, 17, 28–32]. Therefore, additional constraints beyond sliding are needed to properly capture the behavior of real suspensions.

Taking cues from modeling the rheology of dry granular materials [33–37], recent simulations explored how additional stress-activated constraints on rolling affect shear thickening in dense suspensions [38]. Interestingly, under the right conditions, modest increases in rolling friction were found to generate significant effects. At the same volume fraction where suspensions with only sliding constraints exhibit mild shear thickening, adding rolling friction can lead to DST, broaden the stress range over which shear thickening is observed, and increase the viscosity of the frictional state. In Fig. 1B this is shown by comparing the flow curves with (blue) and without (black) rolling friction. In the limit of infinite sliding and rolling friction the frictional jamming point drops as low as $\phi_J^\mu = 0.37$. Short-ranged attractive particle-particle interactions that are not stress-activated and give rise to a yield stress can be included by simply adding them [9], as exemplified by the dashed green trace in Fig. 1B for the case without rolling friction.

Taken together, this opens up an opportunity that we explore here: to model experimental suspension rheology quantitatively and understand how the combination of stress-activated sliding and rolling constraints, expressed in terms of an onset stress for frictional contact and coefficients for sliding and rolling friction, can be linked to particle-scale properties. In principle, additional stress-activated constraints could be included, such as friction that would constrain twisting at particle-particle contacts [35, 39]. However, we find that the contributions of constraints beyond sliding friction, as expressed by the magnitude of the associated friction coefficients, become successively smaller and that an excellent degree of modeling is already achieved by focusing on sliding and rolling friction as the most important ones. We also note that here we consider exclusively constraints that are activated by stress. Of course, similar considerations would hold for constraints, such as particle-particle cohesion, that are deactivated by sufficiently large stress.

To this end we utilize simulations of rigid spheres that include lubrication, electrostatic repulsion, and frictional sliding and rolling constraints. We demonstrate how quantitative detail about the constraints operative over

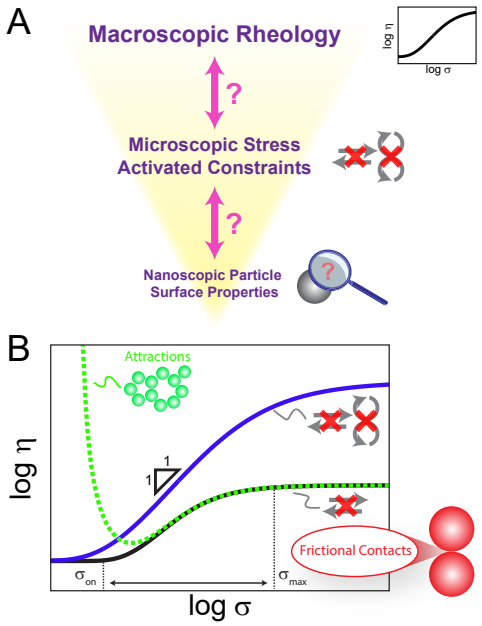

FIG. 1. (A) Shear thickening is a phenomena that can be understood across a hierarchy of length scales, and unraveling the inter-relationship between macroscopic rheology, microscopic stress-activated constraints that hinder relative particle motion, and nanoscopic particle surface properties poses a major challenge. Macroscale rheology can become a sensitive probe of nanometer-scale interactions between particle surfaces once the link with microscopic frictional constraints has been established. (B) How microscopic frictional constraints affect shear thickening. Viscosity η plotted as function of applied shear stress σ at constant volume fraction ϕ. Above the critical onset stress $\sigma_{\rm on}$, "lubricated" contacts are starting to become transformed into "constrained" frictional ones. At $\sigma_{\rm max}$ all contacts are constrained and a maximum plateau viscosity is reached. At this volume fraction, stress-activated sliding constraints alone lead only to continuous shear thickening (*solid black line*). Attractive central forces typically lead to a yield stress, without affecting shear thickening (*dashed green line*). Adding stress-activated rolling constraints can lead to discontinuous shear thickening (DST, slope 1) over a wider stress range and with a higher plateau viscosity (*solid blue line*).

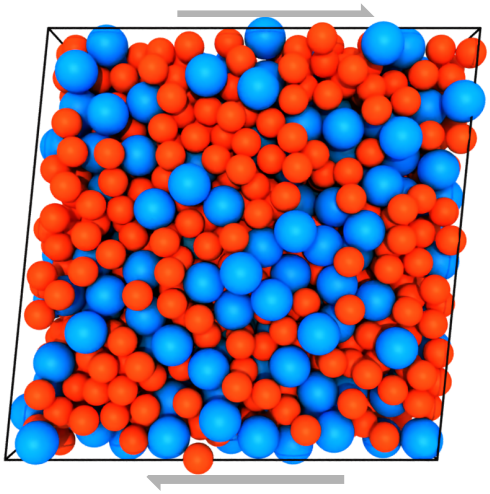

FIG. 2. Unit cell of the simulation, with 2000 total particles of two radii a (red) and 1.4a (blue). Each size particle makes up half of the particle volume fraction. This cell is replicated in all three directions and shearing is imposed by LeesEdwards boundary conditions.

nanoscale distances at particle-particle contacts can be extracted from bulk measurements of $\eta(\sigma)$ as in Fig. 1B by comparing the simulations with experimental data for spherical particles. We first show that a number of commonly studied suspensions that vary widely in their composition, surprisingly have nearly identical frictional constraints and that they primarily affect sliding of contacting particle surfaces. We term these "standard" particle suspensions. We then use the simulations to predict how the magnitudes of stress-activated sliding or rolling friction coefficients alter the relative contributions from the associated constraints to the measured $\eta(\sigma)$ curves. Finally, we illustrate with three examples how modifications to particle surface roughness or chemistry lead to characteristic deviations from the "standard" behavior and how this can be understood in terms of additional stress-activated constraints on particle rolling.

II. METHODS

For all of the experimental systems studied both the Reynolds number and the Stokes number are vanishingly small as they both scale with the square of the particle size [6]. This assumption allows us to simulate particle suspensions in the overdamped limit. We simulate an assembly of inertialess frictional spheres in a Newtonian viscous fluid under an imposed stress σ, that gives rise to an imposed velocity field $\vec{v} = \dot{\gamma}(t)\hat{\vec{v}}(\boldsymbol{x}) = \dot{\gamma}(t)(x_2, 0, 0)$. We use Lees-Edwards periodic boundary conditions with $N = 2000$ particles in a unit cell with a bidisperse particles, with radii a and $1.4a$ mixed at equal volume fractions to avoid ordering [22], as depicted in Fig. 2. The particles interact through short-range hydrodynamic forces (lubrication), short-ranged repulsive forces (electrostatics), and frictional contact forces. The equation of motion for N spheres can be reduced to $6N$-dimensional force (as well as torque) balance between the hydrodynamic ($\vec{F}_{\rm H}$), repulsive ($\vec{F}_{\rm R}$), and contact ($\vec{F}_{\rm C}$) interactions according to:

$$\vec{0} = \vec{F}_{\rm H}(\vec{X}, \vec{U}) + \vec{F}_{\rm C}(\vec{X}) + \vec{F}_{\rm R}(\vec{X}), \tag{1}$$

where $\vec{X}$ and $\vec{U}$ denote the particle positions and velocities/angular velocities, respectively. The leading term in the resistance matrix diverges as $1/h$, with h being the surface-surface distance between particles. We assume the lubrication breakdown below $h_{\rm min} = 0.001a$ (with a being radius of the smaller particle), below which hydrodynamic forces are regularized allowing the particles to come into contact. The electrostatic repulsion used here is representative of a repulsive double-layer electrostatic interaction between particles (mimicking polymer coating, for instance). We model this force as an exponentially decaying with h as $|F_R| = F_0 \exp(-h/\lambda)$, where λ is the Debyle length.

Contacts between particles are modeled using traditional CundallStrack method [40], i.e., using virtual linear springs and we follow algorithm of Luding [39]. We do not use any dashpot explicitly, but in order to stabilize the simulation we make use of lubrication resistance [41]. The contact force between two particles is active only when the surface separation $h < 0$ or overlap $\delta^{(i,j)} \equiv a_i + a_j - |\boldsymbol{r}_i - \boldsymbol{r}_j|$ is positive.

For a particle pair with overlap δ and and center-center unit vector $\boldsymbol{n}$, we compute the normal contact force $\boldsymbol{F}_{\rm C,nor}$, sliding-friction force $\boldsymbol{F}_{\rm C,slid}$, sliding-friction torque $\boldsymbol{T}_{\rm C,slid}$, and rolling-friction torque $\boldsymbol{T}_{\rm C,roll}$ as:

$$\boldsymbol{F}^{(i,j)}_{\rm C,nor} = k_n \delta^{(i,j)} \boldsymbol{n}_{ij} \ , \tag{2a}$$

$$\boldsymbol{F}^{(i,j)}_{\rm C,slid} = k_t \boldsymbol{\xi}^{(i,j)} \ , \tag{2b}$$

$$\boldsymbol{T}^{(i,j)}_{\rm C,slid} = a_i \boldsymbol{n}_{ij} \times \boldsymbol{F}^{(i,j)}_{\rm C,slid} \ , \tag{2c}$$

$$\boldsymbol{T}^{(i,j)}_{\rm C,roll} = a_{ij} \boldsymbol{n}_{ij} \times \boldsymbol{F}^{(i,j)}_{\rm C,roll} \ . \tag{2d}$$

Here, unit vector $\boldsymbol{n_{ij}} \equiv (\boldsymbol{r}_i - \boldsymbol{r}_j)/|\boldsymbol{r}_i - \boldsymbol{r}_j|$ points from particle j to i, and $a_{ij} \equiv 2a_i a_j/(a_i + a_j)$ denotes the reduced radius. Note that $\boldsymbol{F}^{(i,j)}_{\rm C,roll}$

$$\boldsymbol{F}^{(i,j)}_{\rm C,roll} = k_r \boldsymbol{\psi}^{(i,j)} \ , \tag{3}$$

is a quasi-force, which is used only to compute torque, $\boldsymbol{T}^{(i,j)}_{\rm C,roll}$. k_n, k_t and k_r are the normal, sliding and rolling spring constants, respectively. The spring stretches in the sliding and rolling modes are denoted by ξ and ψ, respectively. We chose spring stiffnesses such that the

maximum particle overlaps do not exceed 3% of the particle radius to mimic the rigid limit [25, 42]. The sliding and rolling frictions obey Coulomb's friction laws: $|\boldsymbol{F}^{(i,j)}_{\mathrm{C,slid}}| \leq \mu_s |\boldsymbol{F}^{(i,j)}_{\mathrm{C,nor}}|$ and $|\boldsymbol{F}^{(i,j)}_{\mathrm{C,roll}}| \leq \mu_r |\boldsymbol{F}^{(i,j)}_{\mathrm{C,nor}}|$, with μ_s and μ_r being the sliding and rolling friction coefficients, respectively. Sliding friction was the first contact constraint to be implemented in simulations of dense frictional suspensions [9, 25, 43] and only recently has rolling friction been shown to have a significant effect [38, 44]. Further details on the implementation of sliding and rolling friction can be found in Singh *et al.* [38]. Finally, the total contact force and torque are given by:

$$\boldsymbol{F}^{(i,j)}_{\mathrm{C}} = \boldsymbol{F}^{(i,j)}_{\mathrm{C,nor}} + \boldsymbol{F}^{(i,j)}_{\mathrm{C,slid}} \ , \tag{4a}$$

$$\boldsymbol{T}^{(i,j)}_{\mathrm{C}} = a_i \boldsymbol{n}_{ij} \times \boldsymbol{F}_{\mathrm{C,slid}} + a_{ij} \boldsymbol{n}_{ij} \times \boldsymbol{F}_{\mathrm{C,roll}} \ . \tag{4b}$$

For more information on the simulation method, including the functional forms of the forces in the equations of motion as well how they are solved numerically, we refer the reader to refs. [22, 25, 38]. Unit scales are $\dot{\gamma}_0 \equiv F_0/6\pi\eta_0 a^2$ for the strain rate and $\sigma_0 \equiv \eta_0\dot{\gamma}_0 = F_0/6\pi a^2$ for the stress. The onset stress for shear thickening, σ_{on}, used in the main text is obtained from experimental data and scales as $\sigma_{\mathrm{on}} = \alpha\sigma_0$, with typical values for α around unity.

III. RESULTS

"Standard" particle suspensions: In Fig. 3 we compare the shear thickening behavior across a series of suspension types and volume fractions: sterically stabilized poly(methyl methacrylate) (PMMA) particles in dioctyl phthalate [46], charge stabilized silica particles in aqueous glycerol [47] or PEG-200 [48], glass beads in poly(dimethylsiloxane) (PDMS) [49], and carboxylate-coated particles in aqueous solutions [12, 28]. While the differences in particle size and solvent/surface chemistries do affect the onset stress σ_{on} for shear thickening (see Table I), plotting the reduced viscosity η_r, i.e., η normalized by the viscosity of the suspending liquid, as a function of σ scaled by σ_{on} reveals remarkably similar behavior at each volume fraction, with only a few minor deviations[50] (see Fig. S2 [45] for unscaled data in Fig. 3). Furthermore, these volume-fraction-dependent curves show near quantitative agreement (baseline viscosity values, slope, and extent of shear thickening) with simulations when sliding and rolling friction coefficients were set to $\mu_s = 1$ and $\mu_r = 0$, respectively. In other words, these suspensions can be modeled well even without considering a constraint on rolling. However, with $\mu_s = 1$ this comes at the cost of using a rather large value for the sliding friction coefficient. Our simulations show that this can be remedied and a more physically reasonable $\mu_s = 0.5$ can lead to equally good fits if rolling friction is included by setting $\mu_r = 0.07$. This gives rise to a degeneracy where different combinations of coefficients $\{\mu_s, \mu_r\}$, such as $\{1, 0\}$ produce essentially the same curves of $\eta_r(\sigma)$, will lead to the onset of DST at the same packing fraction of ≈ 0.56, and have the same $\phi^{\mu}_J \approx 0.58$. While this degeneracy makes it impossible for us to extract from the fits precise values for the sliding and rolling friction coefficients $\{\mu_s, \mu_r\}$, it is clear that for these suspensions sliding constraints dominate to a degree that μ_s is significantly larger than μ_r and, as far as the extraction of parameters such as ϕ^{μ}_J is concerned, contributions from rolling friction μ_r can be absorbed in μ_s. We discuss this in more detail in connection with Fig. 4, below.

But first we point out one important aspect in comparing experiments and simulations for large packing fractions ϕ beyond the minimum required for the onset of DST. At such ϕ, stress-controlled shearing conditions throughout the spatial extent of a suspension are very hard to achieve in experiments. This implies that the S-shaped flow curve in plots of shear stress versus shear rate beyond the onset of DST (see Fig. 3, inset) is difficult to map out in experiments, the backward-bending portion typically cannot be accessed, and only a vertical jump in stress is observed (dotted line in the inset). In log-log plots of viscosity versus shear stress (Fig. 3, main panel), this jump appears as a line with slope +1, and experimental data will typically not exceed this slope even deep inside the DST regime. However, the more idealized situation for simulations can trace out the S-shaped curve and produce slopes $\partial(log\eta)/\partial(log\sigma) > 1$. In Fig. 3 for the data shown in black, this discrepancy in the DST regime between simulation data, which appear curved concave downward, and experimental data, which appear as straight lines of slope +1, is therefore due to the inability of conventional rheometry to generate conditions of true stress control inside the suspension [19, 51–54].

All these suspensions are therefore in a regime where their thickening behavior is dictated primarily by sliding constraints. We define these suspensions and others that can be collapsed onto similar sets of $\eta_r(\sigma, \phi)$ curves as "standard" particle suspensions. The key point here is that, while nanometer-scale features and molecular level details at contacting particle surfaces certainly control the interparticle potential (and thus the onset stress), those that modify sliding constraints appear to affect shear thickening most strongly. The collapse of all these experimental data onto the same family of $\eta_r(\sigma, \phi)$ curves and the agreement with the simulations indicates that at each packing fraction

1. the stress-dependent balance of frictional versus lubricated contacts is similar,

2. once particles enter into frictional contact, they experience similar microscopic constraints, and

3. these systems primarily experience constraints on sliding.

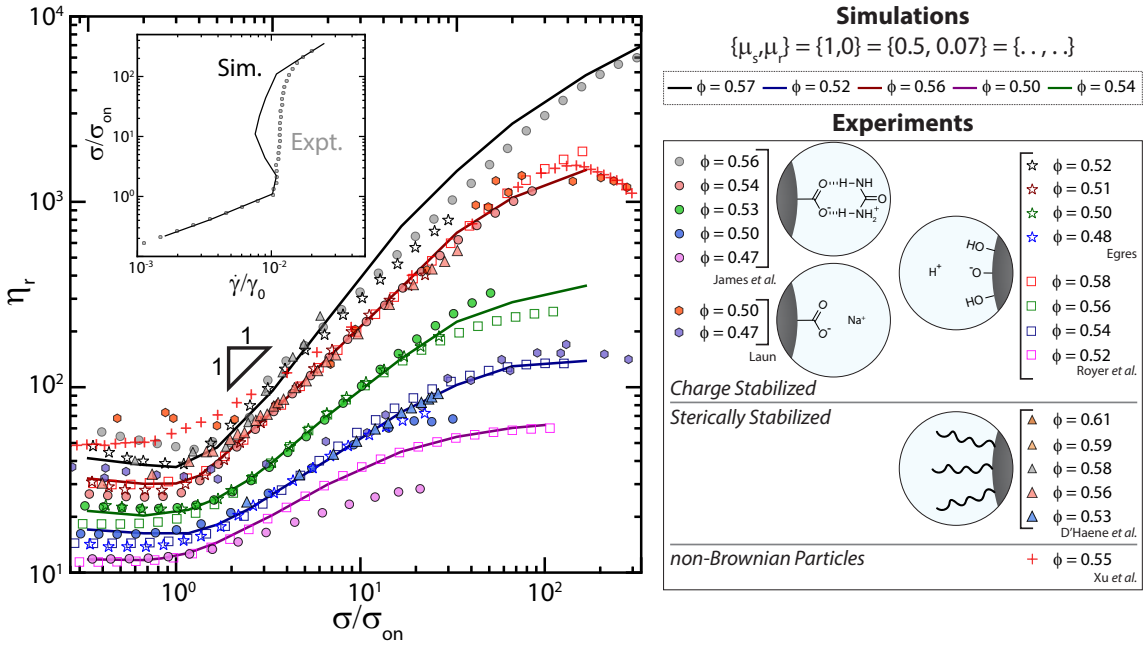

FIG. 3. Shear thickening of "standard" particle suspensions show nearly identical shear thickening after rescaling by the onset stress $\sigma_{\rm on}$. As there are small discrepancies in the experimentally-reported volume fractions, data with similar thickening are grouped by color. See Table I for details regarding particle size, solvent, and onset stress. Solid lines denote simulation data for $\{\mu_s, \mu_r\} = \{0.5, 0.07\}$ and Debye length $\lambda/a = 0.01$ at various volume fractions ϕ as mentioned. (*Inset*) Beyond the onset of DST $\phi_c < \phi < \phi_J^\mu$, simulations (*solid black line*) capture non-monotonic flow curves while experimental measurements cannot (*filled grey circles*). For unscaled data, see Fig. S1 [45].

Particle Identity	Particle size (diameter)	Solvent	Stabilization type	$\sigma_{\rm on}$ (Pa)
PMMA [46]	0.69 μm	dioctyl phthalate	steric	220
Silica [47]	1.54 μm	aqueous glycerol	charge	418
Silica [48]	0.45 μm	PEG-200	charge	433
Carboxylic acid coated Latex [28]	0.20 μm	pH = 6.2 aqueous solution	charge	5.66
Carboxylic acid coated PMMA [12]	0.80 μm	6 M urea in aqueous glycerol	charge	160
Glass [49]	20 μm	low molecular weight PDMS	non-Brownian	1.66

TABLE I. Details of suspension properties in Fig. 3 (see Fig. S1 [45] for determination of $\sigma_{\rm on}$).

Altering Jamming via Microscopic Frictional Constraints: As shown in Ref. [38], the minimum volume fraction ϕ_J^μ required for the onset of jamming depends on both sliding and rolling frictional constraints. In Fig. 4 we show this dependence with data traces at various fixed μ_s while varying μ_r. The set of friction coefficients $\{\mu_s, \mu_r\} = \{0, 0\}$ represents the limit of no microscopic frictional constraints with a jamming point $\phi_J^\mu \approx 0.65$. Conversely, $\{\mu_s, \mu_r\} = \{\infty, \infty\}$ is the limit where relative particle motion at contact is fully constrained (e.g. contacting particles can neither slide nor roll) and $\phi_J^\mu \approx 0.37$.

The data in Fig. 4 provide the context for understanding "standard" particle suspensions as well as deviations from it. The thick horizontal band represents the "standard" particle suspensions shown in Fig. 3, for which the jamming volume fraction $\phi_J^\mu \approx 0.58$. The jamming onset is relatively insensitive to rolling friction as long as $\mu_r < 0.1$ (but the curves do have a small slope as $\mu_r \to 0$, see Figure S2 for Fig. 4 plotted on a linear-linear scale in this region), meaning that friction coefficients for the "standard" particle suspensions could range between $0.5 < \mu_s < 1$ and $0 < \mu_r < 0.07$. This demonstrates that shear thickening data for given ϕ_J^μ in this range can be captured by simulations with no rolling friction but large sliding friction ($\mu_s \approx 1$) or equally well by simulations with appropriately chosen sets of values of rolling friction $0 < \mu_r \leq 0.07$ and sliding friction $0.5 \leq \mu_s < 1$.

While in such sets $\{\mu_s, \mu_r\}$ the rolling friction is always significantly smaller than μ_s, we note that, in absolute terms, even $\mu_r = 0.07$ can be considered large compared to values associated with many tribology experiments on dry particles [55–60]. However, typical tribology experiments consider contacting surfaces that are much more macroscopic and thus surface imperfections are likely to

play a larger role for the suspensions discussed here. Figure 4 also demonstrates that driving $\phi_J^\mu \approx 0.55$, while keeping the sliding friction in the range $\mu_s < 1$, is only possible by adding severe rolling friction $\mu_r > 0.1$ (also see Fig. S2 [45]). For given μ_s, such large amounts of rolling friction lead to steep drop in ϕ_J^μ. This breaks the degeneracy present for "standard" suspensions and allows for a greater opportunity to isolate the two contributions. It explains observations such as $\phi_J^\mu \approx 0.45$ for raspberry-type particles [13] or related findings for other rough particles [29, 31, 32]. Thus in systems with only sliding and rolling constraints, by experimentally determining ϕ_J^μ one can check immediately whether a shear thickening suspension is governed mainly by sliding constraints ("standard") or by a combination of sliding and severe rolling constraints.

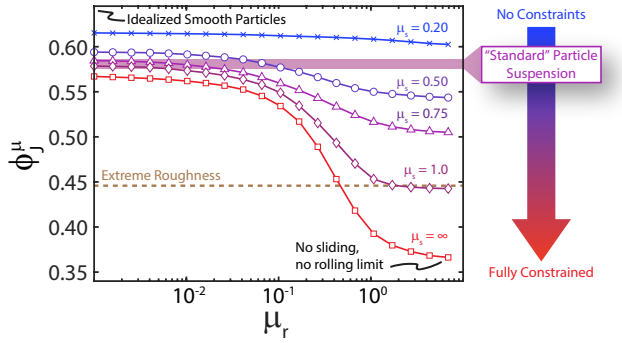

FIG. 4. Tuning the jamming volume fraction map by changing stress-activated frictional constraints due to sliding (μ_s) and rolling (μ_r). The horizontal thick line represents the jamming volume fraction for "Standard" Particle Suspensions, while "Extreme Roughness" refers to the experimentally measured jamming point for rough raspberry-type particles [13].

Deviations from "Standard" Behavior due to Rolling Constraints: We now focus on three illustrative deviations from the "standard" suspension behavior, starting with the most intuitive case, namely very rough particles, where large protruding asperities can interlock as particles come into contact. This reduces the jamming volume fraction significantly [13, 29, 31, 32], and thus in light of Fig. 4 indicates the presence of an additional constraint on rolling.

As an example we show in Fig. 5A data from experiments by Hsiao *et al.* with PMMA particles of increasing roughness, from smooth (SM) and medium rough (MR) to very rough (VR) (with dimensionless asperity sizes of 0.026, 0.075, and 0.082, respectively) at a volume fraction $\phi = 0.5$ [29]. For smooth colloids the distance to jamming $\phi_J^\mu - \phi$ is so large that no shear thickening is expected and $\eta_r(\sigma)$ is essentially flat. For the MR particles the jamming volume fraction was found in the experiments to decrease to $\phi_J^\mu = 0.59$. According to Fig. 4 this implies standard suspension behavior, where combinations of $\{\mu_s, \mu_r\}$ for the limit of dominant sliding friction are appropriate. Specifically, we find that simulations with $\{\mu_s, \mu_r\} = \{0.5, 0\}$ can reproduce the experimental well. However, for the VR colloids the experimentally determined $\phi_J^\mu = 0.54$ cannot be reached simply by increasing sliding friction, even in the limit of infinite μ_s. This is a clear indicator that now the particle surface is sufficiently rough that asperities interlock to constrain also rolling. Based on Fig. 4 we expect that $\eta_r(\sigma)$ for the VR suspensions can be reproduced by increasing $\{\mu_s, \mu_r\} = \{0.5, 0\}$ used for the MR system to combinations such as $\{1, 0.1\}$. This is shown by the red trace in Fig. 5A. We also show in Table S1 [45] the possible combinations of rolling and sliding constraints that are extracted from other literature data [13, 29, 32] of rough particles. This table shows that for suspensions not in the "standard" family (i.e., for $\phi_J^\mu < 0.58$), one can deconvolve the contributions of rolling and sliding friction and extract qualitative trends comparing the relative contributions of each.

Changes in particle surface chemistry have also been shown to affect shear thickening. For example, addition of urea decreases shear thickening in aqueous suspensions of particles coated with carboxylic acid groups (-CO_2H) [12, 14], as shown in Fig. 5B. In this figure the experimental data have been scaled by their respective onset stresses for thickening σ_{on}. Data without added urea (i.e. 0 M) are matched by the simulations only when combinations of sliding and rolling friction are used that fall outside the "standard" range in Fig. 4, such as $\{\mu_s, \mu_r\} = \{0.5, 0.25\}$ or $\{0.6, 0.10\}$. Such large effective friction, resulting from significant constraints on sliding plus additional strong rolling resistance, can be attributed to the formation of hydrogen bonds between carboxylated surfaces as particles are coming into close contact. The reduced shear thickening in 6 M urea is then caused by "capping" of the -CO_2H groups. This disrupts hydrogen bonding, and urea thereby reduces the effective friction coefficient to levels of "standard" suspensions. This is seen by the fact that we can model the 6 M urea data in Fig. 5B with combinations such as $\{\mu_s, \mu_r\} = \{0.5, 0.07\}$.

The constraint-based perspective also sheds new light on the observation that shear thickening for CO_2H-coated latex is highly dependent on pH [28]. At a constant volume fraction, suspensions at pH = 7.1 exhibit continuous shear thickening whereas those at pH = 5.1 display DST (Fig. 5C). While the viscosity of the low stress state of the experimental data is considerably higher than that of the simulation, this is due to the existence of a finite yield stress and shear thinning in the experimental data set (here we only show the data for intermediate to high stress region, full data is shown in Figure S3 [45, 61]). By fixing $\mu_s = 1$ for convenience and increasing rolling constraints μ_r from 0 to 1.0 in the simulations, we can quantitatively reproduce the experimental data- (see Table S1 [45] for other combinations of μ_s and μ_r that can reproduce this experimental dataset). The constraint-based picture therefore allows us to move beyond the results of Noy *et al.* [62], who showed that the

effective friction coefficient between -CO_2H coated surfaces increases with decreasing pH. Specifically, increased hydrogen bonding between "sticky" or adhesive protonated -CO_2H groups at lower pH gives rise to increased sliding and rolling constraints, which are responsible for the changes in the shear thickening behavior observed on macroscopic scales.

CONCLUSIONS

Our numerical simulations highlight the power of a constraint-based approach for understanding and predicting the shear thickening behavior of diverse kinds of dense suspensions, including a wide range of different particle types and particle surface features. We find that two constraints on relative particle movement suffice for quantitative modeling, namely separate constraints on sliding and rolling that are activated when the local stress exceeds a threshold such that particles are coming into direct contact and experience friction forces. A central point in this approach is that each constraint can represent a variety of different physical or chemical interactions giving rise to this friction. In particular, the approach allows one to translate ideas about chemical interactions typically developed under more dilute, closer to equilibrium conditions to these concentrated, out-of-equilibrium systems. In the simulations, constraints are implemented via associated friction coefficients μ_s and μ_r, whose magnitudes provide an indicator of their relative strength. The combination of sliding and rolling constraints can affect the shear thickening behavior in highly nonlinear ways. As Fig. 4 demonstrates, for physically realistic values $\mu_s \approx 0.5$ additional rolling resistance can have a very large effect on ϕ_J^μ and thus on the stress response of a dense suspension. As a result, plots of the suspension viscosity $\eta(\sigma)$ as a function of applied shear stress can be viewed as a macroscopic reporter of stress-activated constraints that originate from contact interactions at the nanoscale. In particular:

- if $\eta(\sigma)$ *follows* the "standard" rheology in Fig. 3, then the rolling and sliding friction coefficients fall within the "flat" region of ϕ_J^μ in Fig. 4, indicating dominant sliding friction. Rolling friction is sufficiently small ($\mu_r < 0.1$) that its effect on the behavior of the suspension viscosity can be subsumed by an enhanced sliding friction coefficient;
- if $\eta(\sigma)$ *deviates* from the "standard" rheology, then the rolling constraints are stronger due to severe surface roughness or stress-activated, "sticky" chemical interactions such as hydrogen bonding between particle surfaces

We note that access to such detailed information about the relative contributions from sliding and rolling is exceedingly difficult to obtain from experiments that use scanning probe techniques, which necessarily focus on lateral sliding motion.

In terms of an effective coefficient of friction accounting for the role of both μ_s and μ_r, the "flat" region of ϕ_J^μ in Fig. 3 provides an explanation as to why prior simulations that did not include rolling friction were still able to model "standard" suspensions as long as they used large values of $\mu_s \approx 1$ [24, 25, 43]. More generally, Fig. 3 shows that combinations of different types and strengths of contact interactions, represented by different sets of values for μ_s and μ_r, can give rise to the same jamming threshold ϕ_J^μ and thus the same shear thickening behavior. Future work could possibly break this degeneracy by measuring and comparing additional bulk rheological properties to simulations, such as the suspensions oscillatory response or normal stress differences which may be more sensitive to μ_r and μ_s. Additionally, this degeneracy could also be broken by considering the range of stresses over which the shear thickening transition occurs, as both polydispersity and rolling friction have been shown to broaden this range [44, 63]. Therefore, our results suggest that ϕ_J^μ suitably represents the combined effect of the two different types of constraint. The same framework could also be adapted to understand how stress-deactivated constraints [18] give rise to shear thinning. Finally, while we here only focused on the connection between microscopic constraints and the macroscopic shear thickening response, there are open questions on how different stress-activated constraints alter the mesoscale force-chain network.

Acknowledgments: We acknowledge support from the Center for Hierarchical Materials Design (CHiMaD) under award number 70NANB19H005 (US Dept. Commerce), and from the Army Research Office under grants W911NF-19-1-0245, W911NF-20-2-0044, and W911NF-21-1-0038.

[1] Philippe Coussot, *Mudflow Rheology and Dynamics* (CRC Press, 1997).
[2] Henri Van Damme, "Concrete material science: past, present, and future innovations," Cem. Concr. Res. **112**, 5–24 (2018).
[3] Elena Blanco, Daniel JM Hodgson, Michiel Hermes, Rut Besseling, Gary L Hunter, Paul M Chaikin, Michael E Cates, Isabella Van Damme, and Wilson C K Poon, "Conching chocolate is a prototypical transition from frictionally jammed solid to flowable suspension with maximal solid content," Proc. Natl. Acad. Sci. USA **116**, 10303–10308 (2019).
[4] Eric Brown and Heinrich M. Jaeger, "Shear thickening in concentrated suspensions: phenomenology, mechanisms

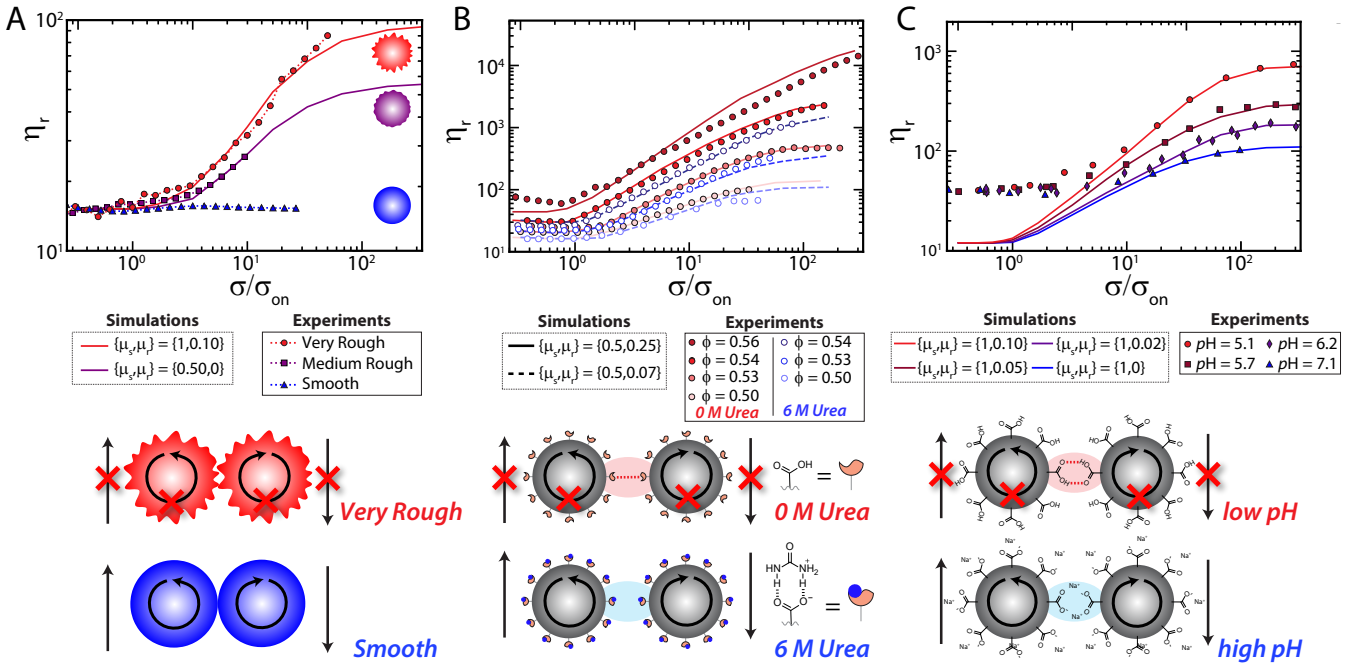

FIG. 5. Linking changes in microscopic constraints to deviations from "standard" behavior. (A) Particle surface roughness modifies both sliding and rolling constraints. Experimental data from Ref. [29] at volume fraction $\phi = 0.5$ (*symbols*) for variable roughness with $\sigma_{on} = 0.95$ Pa (MR) and 5 Pa (VR), simulation data (*lines*) for combinations for $\{\mu_s, \mu_r\}$. (B) Addition of urea to carboxylic acid (-CO_2H) coated particles disrupts interparticle hydrogen bonding and specifically reduces rolling constraints. Experimental data from Ref. [12]. The onset stress σ_{on} for 0 M and 6M urea concentrations is 5 Pa and 160 Pa, respectively. (C) Decreasing solution pH for -CO_2H coated particles dramatically increases microscopic constraints. Experimental data from Ref. [28]. Here, σ_{on} is 3500 (pH=7.1), 1925 (6.2), 696.6 (5.7), and 96.3 (5.1) Pa.

and relations to jamming," Rep. Prog. Phys. **77**, 046602 (2014).

[5] Jeffrey F Morris, "Shear thickening of concentrated suspensions: Recent developments and relation to other phenomena," Annual Review of Fluid Mechanics **52**, 121–144 (2020).

[6] J. Mewis and N. J. Wagner, *Colloidal Suspension Rheology* (Cambridge University Press, 2011).

[7] Morton M Denn, Jeffrey F Morris, and Daniel Bonn, "Shear thickening in concentrated suspensions of smooth spheres in newtonian suspending fluids," Soft Matter **14**, 170–184 (2018).

[8] Élisabeth Guazzelli and Olivier Pouliquen, "Rheology of dense granular suspensions," J. Fluid Mech. **852** (2018).

[9] Abhinendra Singh, Sidhant Pednekar, Jaehun Chun, Morton M Denn, and Jeffrey F Morris, "From yielding to shear jamming in a cohesive frictional suspension," Phys. Rev. Lett. **122**, 098004 (2019).

[10] Safa Jamali and John F Brady, "Alternative frictional model for discontinuous shear thickening of dense suspensions: Hydrodynamics," Phys. Rev. Lett. **123**, 138002 (2019).

[11] Jean Comtet, Guillaume Chatté, Antoine Niguès, Lydéric Bocquet, Alessandro Siria, and Annie Colin, "Pairwise frictional profile between particles determines discontinuous shear thickening transition in non-colloidal suspensions." Nat. Comm. **8**, 15633 (2017).

[12] Nicole M James, Endao Han, Ricardo Arturo Lopez de la Cruz, Justin Jureller, and Heinrich M Jaeger, "Interparticle hydrogen bonding can elicit shear jamming in dense suspensions," Nat. Mater. **17**, 965 (2018).

[13] Chiao-Peng Hsu, Shivaprakash N. Ramakrishna, Michele Zanini, Nicholas D. Spencer, and Lucio Isa, "Roughness-dependent tribology effects on discontinuous shear thickening," Proc. Nat. Acad. Sci. (2018).

[14] Nicole M James, Chiao-Peng Hsu, Nicholas D Spencer, Heinrich M Jaeger, and Lucio Isa, "Tuning interparticle hydrogen bonding in shear-jamming suspensions: Kinetic effects and consequences for tribology and rheology," J. Phys. Chem. Lett. **10**, 1663–1668 (2019).

[15] Philippe Bourrianne, Vincent Niggel, Gatien Polly, Thibaut Divoux, and Gareth H McKinley, "Unifying disparate experimental views on shear-thickening suspensions," arXiv preprint arXiv:2001.02290 (2020).

[16] Mike van der Naald, Liang Zhao, Grayson L Jackson, and Heinrich M Jaeger, "The role of solvent molecular weight in shear thickening and shear jamming," Soft Matter (2021).

[17] Chiao-Peng Hsu, Joydeb Mandal, Shivaprakash N Ramakrishna, Nicholas D Spencer, and Lucio Isa, "Exploring the roles of roughness, friction and adhesion in discontinuous shear thickening by means of thermo-responsive particles," Nature communications **12**, 1–10 (2021).

[18] B M Guy, JA Richards, DJM Hodgson, E Blanco, and W C K Poon, "Constraint-based approach to granular dispersion rheology," Phys. Rev. Lett. **121**, 128001 (2018).

[19] Ivo R Peters, Sayantan Majumdar, and Heinrich M

Jaeger, "Direct observation of dynamic shear jamming in dense suspensions," Nature **532**, 214–217 (2016).
[20] Ryohei Seto, Abhinendra Singh, Bulbul Chakraborty, Morton M. Denn, and Jeffrey F. Morris, "Shear jamming and fragility in dense suspensions," Gran. Matt. **21**, 82 (2019).
[21] Ryohei Seto, Romain Mari, Jeffrey F. Morris, and Morton M. Denn, "Discontinuous shear thickening of frictional hard-sphere suspensions," Phys. Rev. Lett. **111**, 218301 (2013).
[22] Romain Mari, Ryohei Seto, Jeffrey F. Morris, and Morton M. Denn, "Shear thickening, frictionless and frictional rheologies in non-Brownian suspensions," J. Rheol. **58**, 1693–1724 (2014).
[23] B. M. Guy, M. Hermes, and W. C. K. Poon, "Towards a unified description of the rheology of hard-particle suspensions," Phys. Rev. Lett. **115**, 088304 (2015).
[24] Christopher Ness and Jin Sun, "Shear thickening regimes of dense non-Brownian suspensions," Soft Matter **12**, 914–924 (2016).
[25] Abhinendra Singh, Romain Mari, Morton M Denn, and Jeffrey F Morris, "A constitutive model for simple shear of dense frictional suspensions," J. Rheol. **62**, 457–468 (2018).
[26] Cécile Clavaud, Antoine Bérut, Bloen Metzger, and Yoël Forterre, "Revealing the frictional transition in shear-thickening suspensions," Proc. Natl. Acad. Sci. U.S.A. , 5147–5152 (2017).
[27] Matthieu Wyart and Michael E. Cates, "Discontinuous shear thickening without inertia in dense non-Brownian suspensions," Phys. Rev. Lett. **112**, 098302 (2014).
[28] Hans Martin Laun, "Rheological properties of aqueous polymer dispersions," Angew. Makromol. Chem. **123**, 335–359 (1984).
[29] Lilian C Hsiao, Safa Jamali, Emmanouil Glynos, Peter F Green, Ronald G Larson, and Michael J Solomon, "Rheological state diagrams for rough colloids in shear flow," Phys. Rev. Lett. **119**, 158001 (2017).
[30] Lilian C Hsiao and Shravan Pradeep, "Experimental synthesis and characterization of rough particles for colloidal and granular rheology," Curr. Opin. Colloid Interface Sci. (2019).
[31] D. Lootens, Henri van Damme, Y. Hémar, and P. Hébraud, "Dilatant flow of concentrated suspensions of rough particles," Phys. Rev. Lett. **95**, 268302 (2005).
[32] Shravan Pradeep, Mohammad Nabizadeh, Alan R Jacob, Safa Jamali, and Lilian C Hsiao, "Jamming distance dictates colloidal shear thickening," Physical Review Letters **127**, 158002 (2021).
[33] Nicolas Estrada, Emilien Azéma, Farhang Radjai, and Alfredo Taboada, "Identification of rolling resistance as a shape parameter in sheared granular media," Phys. Rev. E **84**, 011306 (2011).
[34] Jun Ai, Jian-Fei Chen, J Michael Rotter, and Jin Y Ooi, "Assessment of rolling resistance models in discrete element simulations," Powder Technology **206**, 269–282 (2011).
[35] Andrew Pablo Santos, Dan S Bolintineanu, Gary S Grest, Jeremy B Lechman, Steven J Plimpton, Ishan Srivastava, and Leonardo E Silbert, "Granular packings with sliding, rolling, and twisting friction," Physical Review E **102**, 032903 (2020).
[36] W Ding, AJ Howard, MD Murthy Peri, and C Cetinkaya, "Rolling resistance moment of microspheres on surfaces: contact measurements," Philosophical Magazine **87**, 5685–5696 (2007).
[37] C Dominik and AGGM Tielens, "Resistance to rolling in the adhesive contact of two elastic spheres," Phil. Mag. A **72**, 783–803 (1995).
[38] Abhinendra Singh, Christopher Ness, Ryohei Seto, Juan J. de Pablo, and Heinrich M. Jaeger, "Shear thickening and jamming of dense suspensions: The "roll" of friction," Phys. Rev. Lett. **124**, 248005 (2020).
[39] S. Luding, "Cohesive, frictional powders: contact models for tension," Gran. Matt. **10**, 235–246 (2008).
[40] P. A. Cundall and O. D. L. Strack, "A discrete numerical model for granular assemblies," Geotechnique **29**, 47–65 (1979).
[41] Romain Mari, Ryohei Seto, Jeffrey F. Morris, and Morton M. Denn, "Nonmonotonic flow curves of shear thickening suspensions," Phys. Rev. E **91**, 052302 (2015).
[42] Abhinendra Singh, Vanessa Magnanimo, Kuniyasu Saitoh, and Stefan Luding, "The role of gravity or pressure and contact stiffness in granular rheology," New J. Phys **17**, 043028 (2015).
[43] Romain Mari, Ryohei Seto, Jeffrey F Morris, and Morton M Denn, "Discontinuous shear thickening in brownian suspensions by dynamic simulation," Proceedings of the National Academy of Sciences **112**, 15326–15330 (2015).
[44] Romain Mari and Ryohei Seto, "Force transmission and the order parameter of shear thickening," Soft Matter **15**, 6650–6659 (2019).
[45] See Supplemental Material for details, which includes Refs. [61].
[46] P. D'Haene, Jan Mewis, and G. G. Fuller, "Scattering dichroism measurements of flow-induced structure of a shear thickening suspension," J. Colloid Interface Sci. **156**, 350–358 (1993).
[47] John R Royer, Daniel L Blair, and Steven D Hudson, "Rheological signature of frictional interactions in shear thickening suspensions," Phys. Rev. Lett. **116**, 188301 (2016).
[48] Ronald G. Egres, *The effect of particle anisotropy on the rheology and microstructure of concentrated colloidal suspensions through the shear thickening transition*, Ph.D. thesis, University of Delaware (2005).
[49] Qin Xu, Abhinendra Singh, and Heinrich M Jaeger, "Stress fluctuations and shear thickening in dense granular suspensions," Journal of Rheology **64**, 321–328 (2020).
[50] There are some discrepancies in the volume fractions, but these are within the typically reported experimental errors associated with determining exact particle density and/or packing fraction [64]. The deviation at low volume fraction for Ref. [12] is because this data was taken at a constant ratio of [urea]:[solvent] (6 M), meaning that the amount of urea relative to the concentration of surface - CO_2H groups changes with packing fraction. The higher relative urea concentration at low packing fractions leads to a lower effective friction coefficient between particle surfaces [14].
[51] Michiel Hermes, Ben M. Guy, Wilson C. K. Poon, Guilhem Poy, Michael E. Cates, and Matthieu Wyart, "Unsteady flow and particle migration in dense, non-Brownian suspensions," J. Rheol. **60**, 905–916 (2016).
[52] Endao Han, Nicole M. James, and Heinrich M. Jaeger, "Stress controlled rheology of dense suspensions using

transient flows," Phys. Rev. Lett. **123**, 248002 (2019).
[53] Brice Saint-Michel, Thomas Gibaud, and Sébastien Manneville, "Uncovering instabilities in the spatiotemporal dynamics of a shear-thickening cornstarch suspension," Physical Review X **8**, 031006 (2018).
[54] Vikram Rathee, Daniel L Blair, and Jeffrey S Urbach, "Localized stress fluctuations drive shear thickening in dense suspensions," Proceedings of the National Academy of Sciences **114**, 8740–8745 (2017).
[55] David Tabor and Philip Bowden, *Friction: An Introduction to Tribology* (Anchor Press, 1973).
[56] Regina Fuchs, Thomas Weinhart, Jan Meyer, Hao Zhuang, Thorsten Staedler, Xin Jiang, and Stefan Luding, "Rolling, sliding and torsion of micron-sized silica particles: experimental, numerical and theoretical analysis," Granular Matter **16**, 281297 (2014).
[57] Bharat Bhushan, *Introduction to Tribology* (Wiley, 2018).
[58] Kenneth Ludema and Oyelayo Ajayi, *Friction, Wear, Lubrication: A Textbook in Tribology* (CRC-Press, 1996).
[59] Markus Preuss Lars-Oliver Heim, Jrgen Blum and Hans-Jrgen Butt, "Adhesion and friction forces between spherical micrometer-sized particles," Phys. Rev. Lett. **83**, 3328 (1999).
[60] D. G. Flom and A. M. Bueche, "Theory of rolling friction for spheres," Journal of Applied Physics **30**, 1725 (1959).
[61] RV More and AM Ardekani, "Unifying disparate rate-dependent rheological regimes in non-brownian suspensions," Physical Review E **103**, 062610 (2021).
[62] Aleksandr Noy, Dmitri V Vezenov, and Charles M Lieber, "Chemical force microscopy," Annual Review of Materials Science **27**, 381–421 (1997).
[63] Ben M Guy, Christopher Ness, Michiel Hermes, Laura J Sawiak, Jin Sun, and Wilson CK Poon, "Testing the wyart–cates model for non-brownian shear thickening using bidisperse suspensions," Soft matter **16**, 229–237 (2020).
[64] Wilson CK Poon, Eric R Weeks, and C Patrick Royall, "On measuring colloidal volume fractions," Soft Matter **8**, 21–30 (2012).